Optics & Laser Technology 196 (2026) 114679

Contents lists available at ScienceDirect

Optics and Laser Technology

journal homepage: www.elsevier.com/locate/optlastec

Full length article

Investigation of the dynamic threshold of a doubly-resonant OPO for squeezed state generation

Shaoping Shi [a,b,1,2], Li Gao [a,2], Li-ang Zheng [a], Xuan Liu [a], Long Tian [a,b], Wei Li [a,b], Yajun Wang [a,b], Wenxiu Yao [a], Qingwei Wang [c], Yaohui Zheng [a,b,*]

[a] State Key Laboratory of Quantum Optics Technologies and Devices, Institute of Opto-Electronics, Shanxi University, Taiyuan 030006, China
[b] Collaborative Innovation Center of Extreme Optics, Shanxi University, Taiyuan 030006, China
[c] School of Sciences, Hangzhou Dianzi University, Hangzhou 310018, China

ARTICLE INFO

Keywords:
Squeezed states
Optical parametric oscillator
Doubly-resonant
Dynamic threshold power

ABSTRACT

Quantum squeezed state is an essential resource for quantum sensing and quantum-information experiments. In addition to the squeezing degree, the threshold power of optical parametric oscillator becomes another focus of generating practical squeezing light source. We propose an optimal dynamic threshold pump power model for the doubly-resonant optical parametric oscillator by thoroughly considering the pump-induced thermal effect, and the squeezing generation result matches well with the theoretical prediction for quantum noise reduction at 1064 nm. In virtue of the series of key technologies including coherent control, doubly-resonant cavity length locking, and high gain balanced homodyne detection, the squeezed state with non-classical noise reduction of 12.2 dB (or 13.0 dB without detecting loss) is achieved with the pump power of 8.5 mW. Our method offers alternative strategy of evaluating and optimizing the squeezing generation system.

1. Introduction

Squeezed light, in which the uncertainty in one of the quadrature is reduced below the shot noise limit (SNL), belongs to the most common nonclassical resource in quantum metrology and quantum sensing [1–6]. Over the past 40 years of painstaking efforts, remarkable enhancements have been witnessed in diverse indicators of the squeezed state. These encompass the squeezing level [7–9], the squeezing bandwidth [10–13], the lowest squeezing frequency [14–17], as well as long-term stability [18–20], among others. Squeezed light has found extensive applications in the realm of advancing precision measurement, including gravitational wave detection [21,22], magnetic field measurement [23], stimulated Raman scattering spectroscopy [24], and biological particle measurement [25]. Across diverse systems, squeezed light has not only been successfully generated in experiment [26–28] but is also progressively advancing towards practical implementation. In virtue of a terahertz-order-broadband waveguide optical parametric amplifier, the continuous-wave 8.3 dB squeezed state have been experimentally achieved [29]. Recently, much effort has gone into engineering scalable implementations of such sources using integrated photonics. A deterministic quantum microcomb in a silica micro resonator on a silicon chip have been demonstrated, with the maximum raw squeezing of 1.6 dB and THz optical span attained [30]. Besides, the deterministic generation of a continuous-variable eight-mode entanglement on an integrated optical chip are realized, where the chip delivers a quantum microcomb that produces multimode squeezed-vacuum optical frequency combs below the threshold [31]. The successful generation of squeezed light within these diverse systems unequivocally attests to the pressing demand for practical and integrated sources of squeezed light.

The optical parametric oscillator (OPO) based on the periodically poled $KTiOPO_4$ (PPKTP) crystal represents one of the most efficient approaches for generating the squeezed state with high squeezing factor. It has consistently maintained the record in terms of squeezing level, up to a value of 15 dB at 1064 nm [7]. One of the important advanced technical approaches is the employment of doubly-resonant OPO. From

* Corresponding author at: State Key Laboratory of Quantum Optics Technologies and Devices, Institute of Opto-Electronics, Shanxi University, Taiyuan 030006, China.
E-mail addresses: ssp4208@sxu.edu.cn, yhzheng@sxu.edu.cn (Y. Zheng).
[1] Co-Corresponding author.
[2] These authors contributed equally to this work.

https://doi.org/10.1016/j.optlastec.2026.114679
Received 11 September 2025; Received in revised form 23 November 2025; Accepted 5 January 2026

singly-resonant to doubly-resonant, the threshold is reduced from several hundred milliwatts (mW) to around dozens of mW, opening up a path for saving pump power, and further improving the locked cavity signal-to-noise ratio [32]. Recently, a strongly squeezed light source with squeezing level exceeding 12 dB has been realized at 1550 nm, where the pump power is approximately 10 mW [15,33,34]. However, a doubly-resonant squeezing resonator needs to simultaneously achieve doubly-resonant, as well as (quasi) phase matching, shrinking the operating window of the light system of squeezed state. The PPKTP absorption for the pump field aggravates the conditions of simultaneous achievement of doubly-resonant and phase matching. Furthermore, comparing with 775 nm as the pump beam, the PPKTP crystal has higher absorption at 532 nm [35,36]. As the pump power increases, the thermal effect caused by intracavity absorption intensifies. It is necessary to adopt targeted precise temperature control in diverse pump power to satisfy the OPO's optimal double resonance conditions. On the other hand, to develop squeezed light sources with a high squeezing factor, it is necessary to simultaneously evaluate the optical losses and phase fluctuation of the system that serves as an optimization avenue [8,37]. And the aforementioned method has been successfully applied to calibrate of photoelectric quantum efficiency [7]. Nevertheless, existing model about squeezed and anti-squeezed quadrature variances that has a constant threshold power [38], cannot perfectly evaluate the optical losses and phase fluctuation of the system, making the optimal process off the track. Especially for the short-wavelength band where the absorption of the nonlinear crystal are more significant, further in-depth analysis and research on this aspect are particularly necessary.

In this manuscript, we present an alternative strategy for optimizing the threshold power model of the doubly-resonant OPO, featuring a quantitative analysis of the dynamic interplay between threshold power and pump power. By fully considering the adverse effects of pump-induced thermal effect, the measurement results of the squeezing factor's dependence on pump power are in good agreement with our theoretical model. Finally, a quantum squeezed state with non-classical noise reduction of 12.2 ± 0.2 dB is experimentally prepared at the pump power of only 8.5 mW. Furthermore, we obtain that the total efficiency $\eta_{tot} = 95.0$ % and the total phase fluctuation $\theta = 5$ mard in the squeezing preparation system. Our work maybe provides an optimized scheme for the development of practical short-wavelength pumped squeezed light sources based on the doubly-resonant OPO.

2. Experimental setup

A schematic of the squeezing experimental setup is shown in Fig. 1. The main laser source is a non-planar ring oscillator (NPRO, from Coherent Inc.) laser with 2.0 W continuous-wave single-frequency output power at 1064 nm. The laser preparations, including spatial-mode improvement, polarization purification, and laser power stabilization are similar to our earlier experiments presented in [39]. Both 1064 mode cleaner (MC) and LO MC adopt the cavity length locking method that extracts error signals at the reflection end, so the later one is eliminated in Fig. 1. The MCs consist of two plane mirrors and one curved mirror with a round-trip length of 436.0 mm, and have a finesse of 310 and a linewidth of 2.2 MHz, resulting in a power transmission of 80 %. The phase modulated signal with the modulation frequency of 42.0 MHz is imprinted on the beam by electro-optic modulator (EOM), which is necessary for controlling the several cavity lengths in the downstream optical path [40].

In virtue of the optical beam splitters, the main laser is divided into several parts. About 100 mW of fundamental beam are inject into second harmonics generator (SHG) for generating the OPO pump light [41]. The OPO consists of a piezo actuated concave mirror and a PPKTP crystal with the dimensions of 1.0 mm × 2.0 mm × 10.0 mm, in the form of a semi-monolithic cavity. The crystal end face with a radius of curvature of 12 mm is coated as high reflectivity for the fundamental and pump field, thus serving as the cavity end mirror. The concave mirror with a

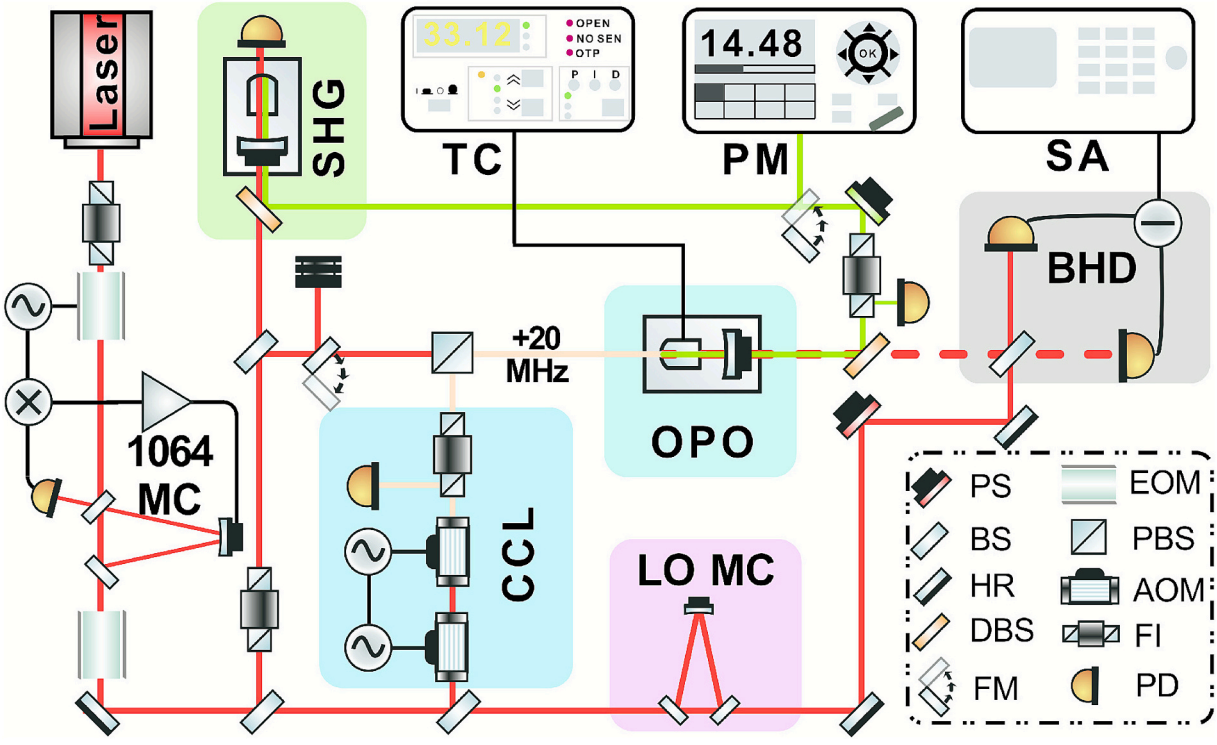

Fig. 1. Setup of the quantum squeezing. PS, Phase shifter; BS, Beam splitter; HR, High reflectivity mirror; DBS, Dichroic beam splitter; FM, Flip mirror; EOM, Electro-optic modulator; PBS, Polarizing beam splitter; AOM, Acousto-optic modulator; FI, Faraday isolator; PD, Photoelectric detector, SHG, Second harmonic generation; OPO, Optical parametric oscillator, MC, Mode cleaner, BHD, Balanced homodyne detector, SA, Spectrum analyzer; TC, Temperature controller; PM, Power meter; CCL, Coherent control loop.

radius of curvature of 25 mm has a transmissivity of 15 ±1.0 % for 1064 nm and 2.5 ± 0.5 % for 532 nm, resulting in the doubly-resonant OPO, which describes a specific optical cavity length where both the pump field and the squeezed light field at the fundamental wavelength are resonant simultaneously. The air gap length between the crystal and the coupling mirror is 22.5 mm, corresponding to a free spectral range (FSR) 3.65 GHz. It should be noted that the modulation frequency (EOM located after 1064 MC, 38 MHz) is smaller than the SHG linewidth, thus the output pump light also carries modulated sidebands at the same modulation frequency, which can be utilized to lock the OPO cavity length. Therefore, no additional pump light phase modulation is required, thus greatly simplifying the complexity of the entire control system. The pump light power that injected into OPO is experimentally measured by the optical power meter (PM, Thorlabs PM100D, S130C). The crystal temperature is stabilized around 33.1 °C to obtain the phase-matching and doubly-resonant condition. By finely tuning the crystal temperature, we ensured simultaneous resonance of the fundamental and pump beams within the cavity.

Approximately 30 mW of the laser beam at 1064 nm serves as the initial alignment of OPO. It is properly blocked by the flip mirror during the squeezed vacuum states generation. We employ two cascade acousto-optic modulators (AOMs) to provide frequency-shifted control field that is 20 MHz away from the main laser. The corresponding reflective field from OPO carries the squeezed angle information inside the OPO cavity. The error signal is obtained by demodulating the photocurrent at twice the beat frequency (40 MHz), feeding back to phase shifter located in the pump path to control the squeezed angle. The squeezed light emitted from the concave mirror is separated from the pump light by a dichroic beam splitter, and carefully mode matched with the local oscillator on a 50/50 beam splitter. By using an auxiliary cavity adjustment technique [9], all of the mode-matching efficiencies in the downstream experiment are significantly improved and reach optimal performance. Fringe visibility between the squeezed beam and local oscillator reaches more than 99.0 %. The output beam from the 50/50 beam splitter is directed toward a balanced homodyne detector (BHD) to observe the quantum noise level. The relative phase between the squeezed field and local oscillator is actively controlled by utilizing the coherent control scheme [42], where the necessary error signal is obtained from demodulating a part of the BHD AC signal with a 20 MHz sinusoidal signal.

For an ideal OPO below the threshold, the squeezed and anti-squeezed quadrature variances can be expressed as [7]:

$$V_{s/a} = [1 \mp \eta_{\mathrm{tot}} \frac{4\sqrt{P/P_{\mathrm{th}}}}{(1 \pm \sqrt{P/P_{\mathrm{th}}})^2 + 4(2\pi f/\gamma)^2}]\cos^2\theta + [1 \pm \eta_{\mathrm{tot}} \frac{4\sqrt{P/P_{\mathrm{th}}}}{(1 \mp \sqrt{P/P_{\mathrm{th}}})^2 + 4(2\pi f/\gamma)^2}]\sin^2\theta \quad (1)$$

where P is the pump power, P_{th} is the threshold power, θ is the phase fluctuation, η_{tot} is the total detection efficiency, γ is the cavity decay rate, and f is the Fourier frequency. In general, based on the above formula and in conjunction with the measured squeezing/anti-squeezing noise spectrum alongside the variation in pump power, the overall system loss and phase fluctuation can be derived [7,39]. For singly-resonant OPO systems, the method described above is universally applicable. However, in the case of doubly-resonant OPO systems, this approach presents specific technical challenges. Thermal effects induced by the pump light field necessitate fine tuning of the temperature controller to achieve optimal doubly-resonant operation of the OPO cavity at varying pump powers. Such variations in crystal temperature, in turn, alter the phase mismatch, causing the OPO threshold to dynamically shift. Therefore, the conventional fitting method that relies on a fixed threshold becomes unsuitable for accurate characterization.

We further analyzed the thermal absorption of the pump field by the crystal. The pump light interacts with the nonlinear crystal via second-order nonlinearity to generate squeezed light. The temperature distribution within a nonlinear crystal, influenced by thermal absorption, is described by a thermal distribution model, and its analytical solution is given by [43]:

$$K_c(x,y) = \sum_{n=1}^{\infty}\sum_{m=1}^{\infty} A_{nm}\sin\frac{n\pi}{a}x\sin\frac{m\pi}{b}y \quad (2)$$

The A_{nm} is a coefficient that related to the OPO intracavity circulating pump power P_{circ}, which can be expressed as:

$$A_{nm} = \frac{4P_{circ}\beta ab}{\chi\pi^2(b^2n^2 + a^2m^2)}\int_0^b\int_0^a \exp\left[-2\frac{(x-a/2)^2 + (y-b/2)^2}{w_p^2}\right]\sin\frac{n\pi}{a}x\sin\frac{m\pi}{b}y dxdy \quad (3)$$

$$P_{circ} = \frac{PL_p}{\left[1 - \sqrt{(1-L_p)(1-V_p)(1-\Gamma_p P_{circ})}\right]^2} \quad (4)$$

In Eqs. (3) and (4), the χ is the thermal conductivity of the crystal, β is the laser absorption rate of the crystal, w_p is the waist size of the pump beam, a and b are the length and width of the end face about the crystal, n and m represent positive integers. Besides, the L_p, V_p, and Γ_p represent the pump transmittance of OPO coupling mirror, the pump round-trip loss, and the pump nonlinear loss, respectively. By solving Eqs. (2)-(4) simultaneously, we obtain the theoretical distribution model of the OPO temperature field. The internal temperature of the crystal increases commensurately with the injected pump power. To achieve maximum squeezing, careful adjustment of the high-precision temperature controller (TC, Thorlabs, TED200C) is essential for each pump power to ensure continuous satisfaction of quasi-phase matching and optimal double-resonance conditions. As shown in Fig. 2, the temperature values of the OPO crystal were determined for pump powers ranging from 1 mW to 10 mW (with 1 mW increments) using theoretical calculations (red dots) and experimental measurements (orange dots). Subsequently, a linear fit was performed on both the theoretical and experimental data to establish the relationship between the crystal temperature and the input pump power, which is expressed as:

$$T1\,(P) = 60.37\,(\pm 1.08)^\circ C/\mathrm{W}\cdot P + 33.25(\pm 0.0067)^\circ C \quad (5)$$

$$T2(P) = -22.74\,(\pm 0.39)^\circ C/\mathrm{W}\cdot P + 33.23(\pm 0.0024)^\circ C \quad (6)$$

The region bounded by the two linear fit curves in Fig. 2 delineates the potential range for the actual crystal temperature as a function of the injected pump power. Within this range, we select the average operating temperature of the crystal as a reasonable assumption for evaluating the dynamic threshold. Under this assumption, we then fit the resulting dynamic-threshold model to the experimentally measured squeezing and anti-squeezing levels, thereby inferring an explicit functional relationship between the crystal temperature and the pump power, given by:

$$T_{\mathrm{act}}(P) = 35.00^\circ C/\mathrm{W}\cdot P + 33.26^\circ C \quad (7)$$

which corresponds to the gray dotted line in Fig. 2. Furthermore, the threshold pump power of doubly-resonant OPO can be expressed as [44]:

$$P_{th} = \frac{(L_p + V_p)^2(L_s + V_s)^2}{8EL_p} \quad (8)$$

$$E = \frac{4\mu_0 d_{eff}^2\omega_s^2\omega_i^2 lh}{\pi c^2 n_p^2\omega_p} \quad (9)$$

$$h = \frac{1}{4\xi}\int\int_{-2\xi}^{0}\frac{\exp[i\Delta k z_R(t-t')]}{(1-it)(1+it') - \zeta^2(1+it)(1-it')}dtdt' \quad (10)$$

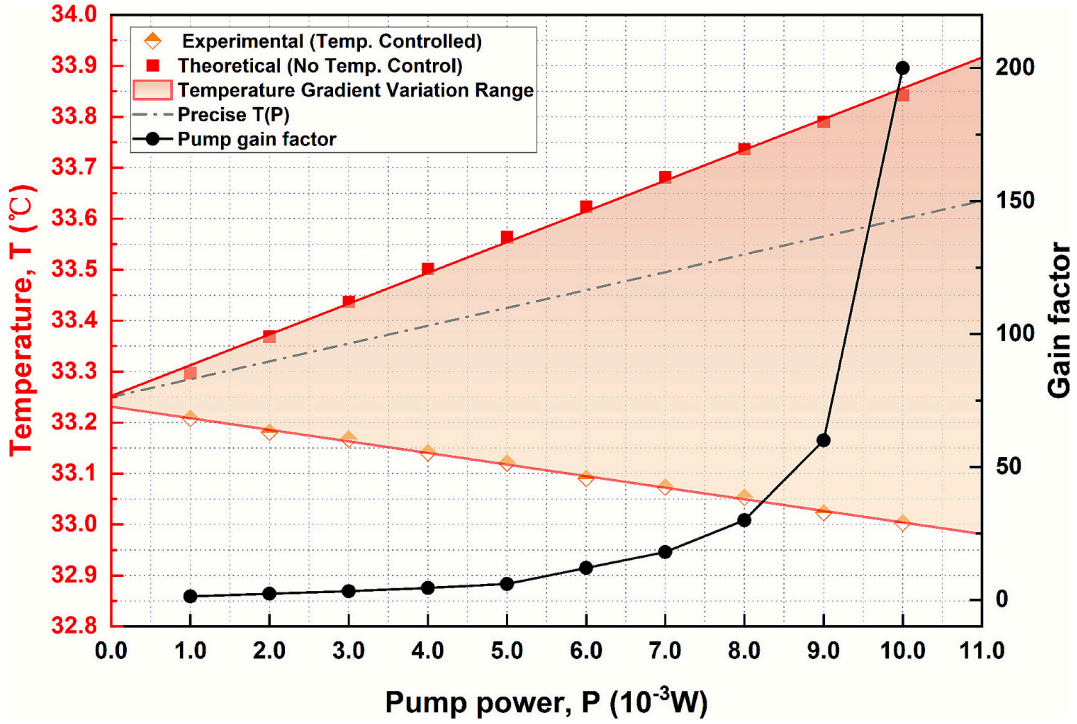

Fig. 2. Pump power dependence of crystal temperature and nonlinear gain coefficient. The x-axis represents the injected pump power. The left y-axis displays the crystal temperature, showing both experimentally measured data (orange points, as indicated by a high-precision temperature controller) and theoretically calculated data (red points, in the absence of external temperature control). The region between the linear fitting curves for these two temperature trends represents the range of variation of the crystal's internal temperature gradient. The gray dotted line represents the precise $T(P)$ for the experimental system. The right y-axis presents the corresponding nonlinear gain coefficient (black points).

where E denotes the nonlinearity; h represents the focused Gaussian light factor, its value is determined by the focusing parameter $\xi = \frac{l}{z_R}$; z_R is Rayleigh range of the cavity mode: $z_R = \frac{n_p \omega_p w_p^2}{2c}$; w_p is the pump beam waist.; ζ is normalized oscillation frequency: $\zeta = 1 - \frac{n_i \omega_i}{n_p \omega_p}$.

And, caused by the temperature derivative of refractive indices (thermo-optical coefficient), the phase-mismatch Δk is dependent on the actual temperature T:

$$\Delta k(T) = \frac{2\pi n_p(T)}{\lambda_p} - \frac{2\pi n_s(T)}{\lambda_s} - \frac{2\pi n_i(T)}{\lambda_i} - \frac{2\pi}{\Lambda} \tag{11}$$

$$\begin{aligned} n_p(T) &= n_p + \Delta n_p T_{act}(P) \\ n_s(T) &= n_s + \Delta n_s T_{act}(P) \\ n_i(T) &= n_i + \Delta n_i T_{act}(P) \end{aligned} \tag{12}$$

The detailed parameters are listed in Table 1.

Take into account the Eqs. (7)-(10), we finally obtain the dependence between P_{th} and P shown in Fig. 3, which can be simply fitted as:

$$P_{th}(P) = (0.0058 \times e^{-P/0.0294} + 0.0068)\ \mathrm{W} \tag{13}$$

To briefly summarize the evolution process, as the injected pump power varies, the actual crystal temperature, influenced by both thermal absorption effects and external temperature control, deviates from its initial value, which consequently alters the temperature-dependent phase mismatch $\Delta k(T)$. A dependency between the dynamic threshold pump power P_{th} and the injected pump power P is thus established via $\Delta k(T)$ and $T(P)$, as presented in Eq. (11). By utilizing Eq. (11), we can determine the OPO threshold corresponding to different pump powers, effectively compensating for the inability to real-time measure threshold power under varying pump conditions. Consequently, this method holds significant importance for predicting thresholds in short-wavelength doubly resonant OPOs, as such devices typically exhibit more pronounced thermal effects.

Table 1
Detailed parameters of P_{th} and E.

Parameters	Definitions	Value
L_p, L_s	Transmittance of coupling mirror	0.025, 0.15
V_p, V_s	Round-trip loss	0.004, 0.002
μ_0	Magnetic permeability	$4\pi \times 10^{-7}$H/m
c	Light speed in vacuum	3.0×10^8 m/s
$\omega_s = \omega_i$, ω_p	Angular frequency	1.77068×10^{15} rad/s, 3.54135×10^{15} rad/s
$\lambda_s = \lambda_i$, λ_p	Wavelength	1.064×10^{-6} m, 0.532×10^{-6} m
$n_s = n_i$, n_p	Refractive index ($T = 25$℃)	1.8302, 1.8894 [45]
$\Delta n_s = \Delta n_i \Delta n_p$	Temperature derivative of the refractive index	3.40×10^5 ℃$^{-1}$, 4.27×10^5 ℃$^{-1}$ [45]
l	Length of crystal	0.01 m
d_{eff}	Effective nonlinear coefficient	10.8×10^{-12} m/V
Λ	Poling period of PPKTP	9.0×10^{-6} m

3. Experimental result

Pump power dependence of the squeezing and anti-squeezing spectra are shown in Fig. 4(a). The squeezing and anti-squeezing factors are repeatedly more 20 times measured at several pump powers. And before each measurement, the temperature controller was finely adjusted to ensure that every data point was taken under optimal operating conditions. All values are directly detected by the spectrum analyzer from zero-span measurements at the analysis frequency of 1 MHz, which are still including electronic noise and normalized to the vacuum noise. The measured squeezing/anti-squeezing noise exhibits excellent agreement with the optimized dynamic threshold model, as the blue solid line in Fig. 4(a). In addition, we introduced two sets of fixed-threshold parameters (11 mW and 14 mW) for comparative fitting analysis. Although the experimentally measured threshold of the OPO is 12 mW, the corresponding fixed-threshold fitting curve exhibits noticeable deviations

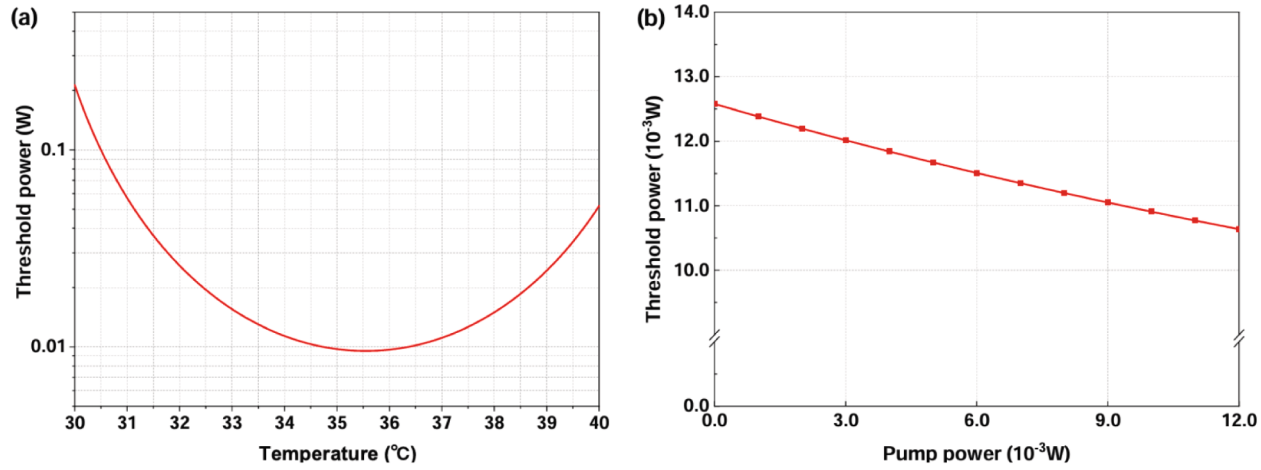

Fig. 3. Dynamic theoretical threshold pump power P_{th} dependence on the (a) temperature T and (b) injected pump power P.

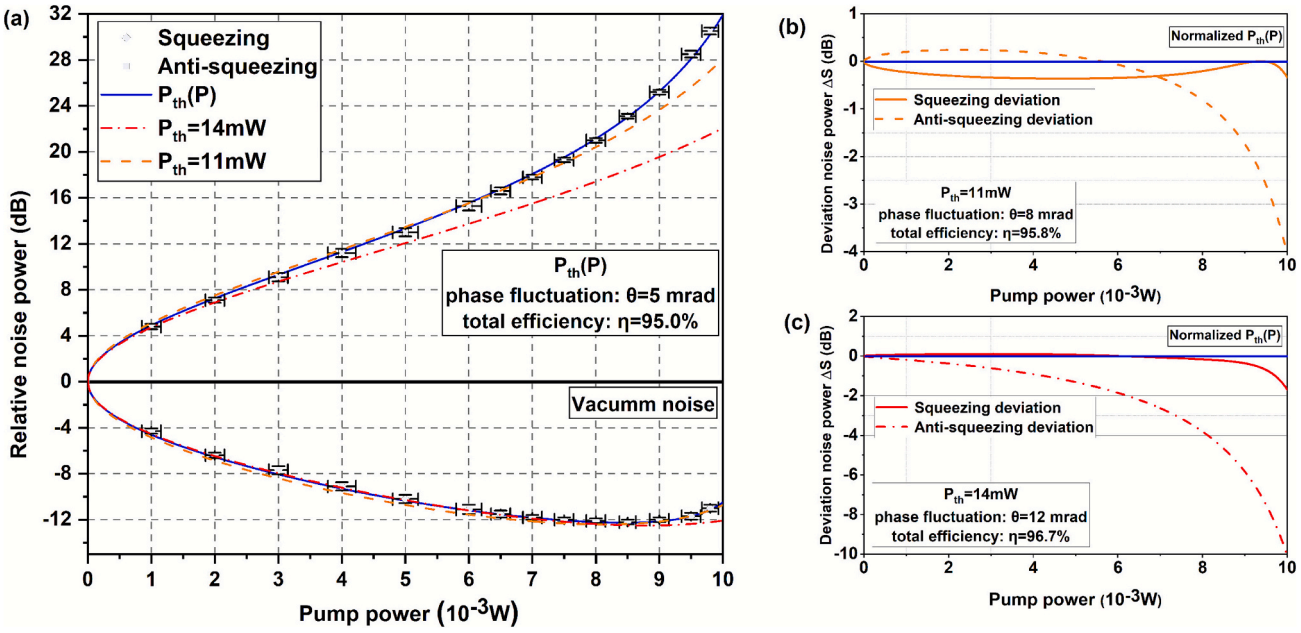

Fig. 4. Characterization of squeezed and anti-squeezed noise evolution with pump power. (a) Squeezing noise and anti-squeezing noise verse pump power at the analysis frequency of 1 MHz. The orange-dash line is the theoretical fixed pump power of 11 mW, meanwhile red-dash-dot line represent that of 14 mW. The blue-solid line denotes the dynamic pump power of $P_{th}(P)$. (b) Deviation values ΔS between the fitted curves for dynamic $P_{th}(P)$ and for a fixed $P_{th} = 11$ mW. The blue solid line shows the normalized dynamic $P_{th}(P)$ fitted curve. The orange solid and dashed lines represent the deviations for squeezing and anti-squeezing, respectively. (c) Deviation values ΔS between the fitted curves for dynamic $P_{th}(P)$ and for a fixed $P_{th} = 14$ mW. The red solid and dashed lines represent the deviations for squeezing and anti-squeezing, respectively. Phase fluctuation and total efficiency obtained under different fitting conditions are also indicated in inset (a), (b), and (c), respectively.

in both the low- and high-pump-power regions. We therefore chose 11 mW and 14 mW as reference thresholds, which yield the best fixed-threshold fitting performance in the high- and low-pump-power regions, respectively. It can be seen that the optimal curve of anti-squeezing gradually transitions from the high threshold line to the low threshold line and crosses the latter. Similar situations also exist for the squeezing noise curve. To further illustrate the discrepancy, Figs. 4(b) and 4(c) present fitting difference plots between the dynamic and fixed thresholds, where the fixed threshold's fitted curves are normalized to $P_{th}(P)$. Fitting the measurement results to different threshold models, we yielded distinct values for both phase fluctuation and total efficiency. Notably, the fitting results derived from the optimized dynamic threshold model offer a more accurate assessment of the system's actual parameters compared to the conventional fixed-threshold model. Finally, we obtain the total efficiency $\eta_{tot} = 95.0$ % and the total phase fluctuation $\theta = 5$ mard.

The Fig. 5 shows the balanced homodyne measurements of the quadrature noise variances at pump power of 8.5 mW with a RBW of 300 kHz and a VBW of 200 Hz. The black trace corresponds to the shot noise of 10 mW local oscillator and is measured with the squeezed light blocked. By linear scanning the LO phase with triangular wave signal, the orange line is presented the quantum noise in the orthogonal quadrature. The smooth and continuous noise curve serves as an indirect reflection of the system's stability. In virtue of the coherent control scheme, we also achieved the squeezing(anti-squeezing) noise measurement by locking the LO phase to the 0 ($\pi/2$), shown in red (blue) line of Fig. 5. It should be pointed out that these three lines show the 10 times average measurements value. The maximum quantum squeezing noise

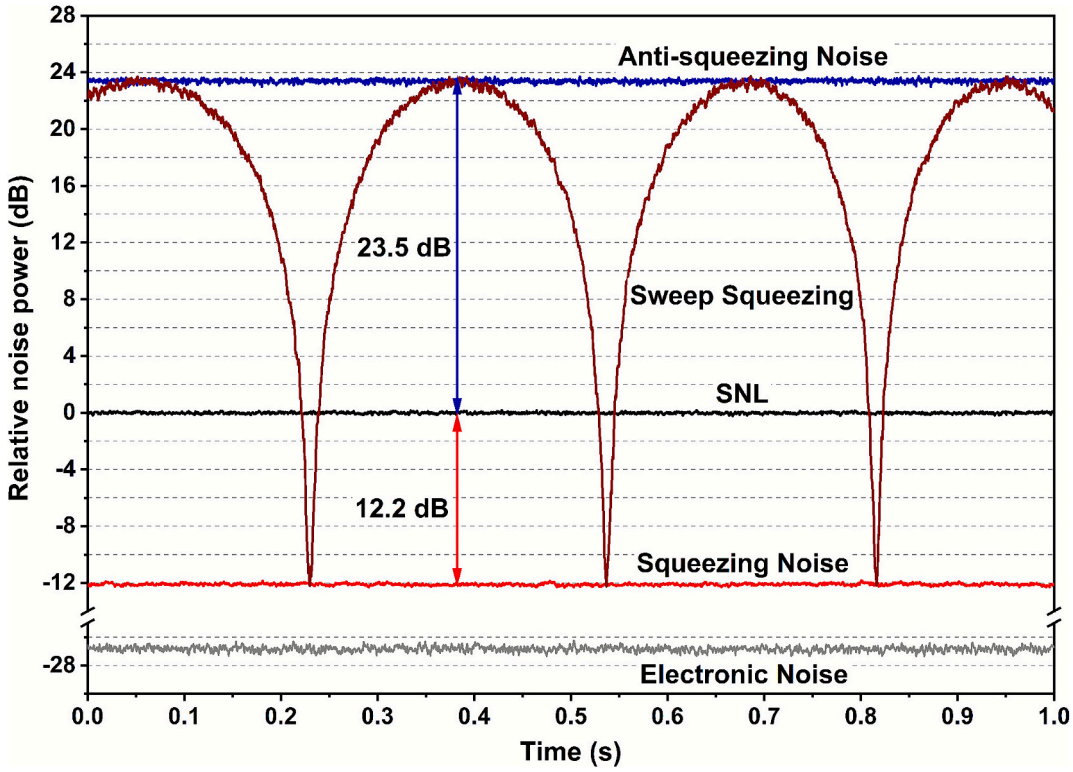

Fig. 5. Normalized quantum noise variances are recorded at the analysis frequency of 1 MHz. RBW of 300 kHz and a VBW of 200 Hz. The 10 times average measurements of SNL, squeezing and anti-squeezing noise are presented.

reduction about 12.2 dB have been directly detected, meanwhile the anti-squeezing noise is 23.5 dB higher than the SNL. Inferring the system's detection loss from the theoretically predicted total efficiency and phase fluctuation, we ultimately achieved a squeezing level of approximately 13.0 dB.

Indeed, another commonly employed OPO configuration is the bow-tie cavity. Compared with a standing-wave OPO, the "single-pass" nature of the intracavity field in a traveling-wave cavity leads to weaker thermally induced effects than the "double-pass" field in a standing-wave cavity. [46–48]. In addition, the bow-tie cavity is often combined with a wedged nonlinear crystal and segmented heating scheme, which not only enables simultaneous optimization of the double-resonance and phase-matching conditions [15], but also suppresses backward-propagating fields, thereby reducing low-frequency parasitic interference noise [49]. Notably, several factors govern the overall thermal behavior of the system, namely the cavity geometry, mirror properties, and the crystal's absorption coefficient. On the other hand, the bow-tie configuration typically introduces higher round-trip losses, which in turn increase the OPO threshold power. Consequently, in practical experiments, the design of the OPO cavity configuration must balance multiple considerations, including thermal effects, intracavity losses, and threshold requirements. The simple-structured semilithic OPO in the experiment helped us to attain maximum measured squeezing levels of 12.2 dB at 1 MHz. By incorporating the OPO coupling mirrors with lower transmittance, we expect to further reduce the required pump power while maintaining the same squeezing factor. Within this improvement methods of generating high-level squeezing source, the provided dynamic threshold model and corresponding fitting process will play a more important role.

4. Conclusion

In conclusion, we have experimentally generated a squeezed state exhibiting non-classical noise reduction of 12.2 ± 0.2 dB, achieved with only 8.5 mW of pump power. We measured squeezing and anti-squeezing across various pump powers and fitted the experimental data using different theoretical models to evaluate system loss and phase fluctuation. The results demonstrate a high degree of consistency between the experimental data and the predictions of our proposed dynamic threshold model, thus validating its effectiveness in characterizing squeezing systems. Besides, the low-threshold OPO architecture and dynamic threshold model offer a viable pathway for realizing efficient and reliable quantum light sources under low-power conditions. This is particularly relevant for squeezed-state systems experiencing significant thermal effects under short-wavelength pumping (such as those pertinent to atomic systems), accurate modeling and performance optimization of squeezed light sources in such systems hold significant research value [50,51]. Furthermore, the ability to operate at low pump power contributes to the advancement of squeezed light sources towards high efficiency and integration. Future improvements can involve selecting low-absorption nonlinear crystals and low-transmittance [34] output couplers to further reduce pump power and enhance the squeezing level.

CRediT authorship contribution statement

Shaoping Shi: Writing – original draft, Validation, Supervision, Investigation, Conceptualization. **Li Gao:** Formal analysis, Data curation. **Li-ang Zheng:** Data curation. **Xuan Liu:** Data curation. **Long Tian:** Resources. **Wei Li:** Formal analysis, Data curation. **Yajun Wang:** Validation, Supervision. **Wenxiu Yao:** Methodology. **Qingwei Wang:** Formal analysis, Conceptualization. **Yaohui Zheng:** Writing – review & editing, Supervision.

Funding

This work is supported by the National Natural Science Foundation of China (Grants No. 62225504, No. 62027821, No. U22A6003, No.

12304399, No. 12174234, and No. 12274275 and No. 62375162); Key R&D Program of Shanxi (Grant No. 202302150101004); Fundamental Research Program of Shanxi Province (Grants No. 202303021212003, and No. 202303021224006).

Declaration of competing interest

The authors declare that they have no known competing financial interests or personal relationships that could have appeared to influence the work reported in this paper.

Data availability

Data will be made available on request.

References

[1] L. A. Wu, et al., Generation of Squeezed States by Parametric Down Conversion. Phys. Rev. Lett. 57, 2520-2523 247 (1986).
[2] M. Tse, et al., Quantum-enhanced advanced LIGO detectors in the era of gravitational-wave astronomy, Phys. Rev. Lett. 123 (2019) 231107.
[3] D. Ganapathy, et al., Broadband quantum enhancement of the LIGO detectors with frequency-dependent squeezing, Phys. Rev. X 13 (2023) 041021.
[4] E.D. Herbschleb, et al., Low-frequency quantum sensing, Phys. Rev. Applied 18 (2022) 034058.
[5] J. Zopes, et al., High-resolution quantum sensing with shaped control pulses, Phys. Rev. Lett. 119 (2017) 260501.
[6] S.P. Shi, et al., Continuous variable quantum teleportation network, Laser Photonics Rev. 17 (2023) 2200508.
[7] H. Vahlbruch, et al., Detection of 15 dB squeezed states of light and their application for the absolute calibration of photoelectric quantum efficiency, Phys. Rev. Lett. 117 (2016) 110801.
[8] S.P. Shi, et al., Detection and perfect fitting of 13.2 dB squeezed vacuum states by considering green-light-induced infrared absorption, Opt. Lett. 43 (2018) 5411–5414.
[9] X.C. Sun, et al., Detection of 13.8 dB squeezed vacuum states by optimizing the interference efficiency and gain of balanced homodyne detection, Chinese Optics Lett. 17 (2019) 072701.
[10] S.P. Shi, et al., Demonstration of channel multiplexing quantum communication exploiting entangled sideband modes, Phys. Rev. Lett. 125 (2020) 070502.
[11] M. Mehmet, et al., Observation of squeezed states with strong photon-number oscillations, Phys. Rev. A 81 (2010) 013814.
[12] S.P. Shi, et al., Generation of entangled sideband modes for frequency multiplexing quantum communication, Journal of Quantum Optics 30 (2024) 040102.
[13] Y.M. Wu, et al., Generating a bandwidth-tunable squeezed state via phase manipulation of entangled sideband modes, Phys. Rev. Applied 23 (2025) 044021.
[14] L. Gao, et al., Generation of squeezed vacuum state in the millihertz frequency band, Light Sci. Appl. 13 (2024) 294.
[15] F. Meylahn, et al., Squeezed states of light for future gravitational wave detectors at a wavelength of 1550 nm, Phys. Rev. Lett. 129 (2022) 121103.
[16] W.H. Yang, et al., Dependence of measured audio- band squeezing level on local oscillator intensity noise, Opt. Express 25 (2017) 24262–24271.
[17] M. Mehmet, H. Vahlbruch, High-efficiency squeezed light generation for gravitational wave detectors, Class. Quantum Grav. 36 (2019) 015014.
[18] B. Shajilal, et al., 12.6 dB squeezed light at 1550 nm from a bow-tie cavity for long-term high duty cycle operation, Opt. Express 30 (2022) 37213–37223.
[19] A. Khalaidovski, et al., Long-term stable squeezed vacuum state of light for gravitational wave detectors, Class. Quantum Grav. 29 (2012) 075001.
[20] H. Grote, et al., First long-term application of squeezed states of light in a gravitational-wave observatory, Phys. Rev. Lett. 110 (2013) 181101.
[21] A. Buikema, et al., Sensitivity and performance of the advanced LIGO detectors in the third observing run, Phys. Rev. D 102 (2020) 062003.
[22] J. Lough, et al., First demonstration of 6 dB quantum noise reduction in a kilometer scale gravitational wave observatory, Phys. Rev. Lett. 126 (2021) 041102.
[23] B.B. Li, et al., Quantum enhanced optomechanical magnetometry, Optica 5 (2021) 850–856.
[24] R.B. de Andrade, et al., Quantum-enhanced continuous-wave stimulated Raman scattering spectroscopy, Optica 7 (289) (2021) 470–475.
[25] M.A. Taylor, et al., Biological measurement beyond the quantum limit, Nat. Photonics 7 (2013) 229–233.
[26] R.E. Slusher, et al., Observation of squeezed states generated by four-wave mixing in an optical cavity, Phys. Rev. Lett. 55 (2016) 2409–2412.
[27] K. Schneider, et al., Generation of strongly squeezed continuous-wave light at 1064 nm, Opt. Express 2 (1998) 59–64.
[28] H. Vahlbruch, et al., Observation of Squeezed Light with 10-dB Quantum-Noise Reduction. Phys. Rev. Lett. 100, 295 033602 (2008).
[29] T. Kashiwazaki, et al., Over-8-dB squeezed light generation by a broadband waveguide optical parametric amplifier toward fault-tolerant ultra-fast quantum computers, Appl. Phys. Lett. 122 (2023) 234003.
[30] Y. Zhang, et al., Squeezed light from a nanophotonic molecule, Nat. Commun. 12 (2023) 2233.
[31] X. Jia, et al., Continuous-variable multipartite entanglement in an integrated microcomb, Nature 639 (2023) 329–336.
[32] J.P. Wang, et al., Design of optical parametric cavity for broadband squeezed light field, Acta Phys. Sin. 69 (2020) 234204.
[33] W.H. Zhang, et al., Optimization of the squeezing factor by temperature-dependent phase shift compensation in a doubly resonant optical parametric oscillator, Appl. Phys. Lett. 115 (2019) 171103.
[34] A. Schonbeck, et al., 13 dB squeezed vacuum states at 1550 nm from 12 mW external pump power at 775 nm, Opt. Lett. 43 (2018) 110–113.
[35] R. Jin, et al., Thermal effects of the quantum states generated from the isomorphs of PPKTP crystal, Opt. Laser Technol. 109 (2019) 222–226.
[36] J.D. Bierlein, et al., Potassium titanyl phosphate: properties and new applications, J. Opt. Soc. Am. B 6 (1989) 622–633.
[37] S. Dwyer, et al., Squeezed quadrature fluctuations in a gravitational wave detector using squeezed light, Opt. Express 301 (21) (1998) 19047–19060.
[38] E.S. Polzik, et al., Atomic spectroscopy with squeezed light for sensitivity beyond the vacuum-state limit, Appl. Phys. B 55 (1992) 279–290.
[39] W. Yang, et al., Detection of stably bright squeezed light with the quantum noise reduction of 12.6 dB by mutually compensating the phase fluctuations, Opt. Lett. 42 (2017) 4553–4556.
[40] R.W.P. Drever, et al., Laser phase and frequency stabilization using an optical resonator, Appl. Phys. B 31 (1983) 97–105.
[41] W. Yao, et al., Realizing high efficiency 532 nm laser by optimizing the mode-and impedance-matching, Laser Phys. Lett. 18 (2021) 015001.
[42] H. Vahlbruch, et al., Coherent control of vacuum squeezing in the gravitational-wave detection band, Phys. Rev. Lett. 97 (2006) 011101.
[43] L. Li, et al., Temperature field of quadrate frequency crystal KTP in all-solid–statelaser, Laser Technology 29 (2018) 350–353.
[44] S. Schiller, K. Schneider, J. Mlynek, Theory of an optical parametric oscillator with resonant pump and signal, J. Opt. Soc. Am. B 16 (1999) 1512–1524.
[45] V.G. Dmitriev, G.G. Gurzadyan, D.N. Nikogosyan, Handbook of nonlinear optical crystals (3rd ed), Springer, Berlin, Germany, 1999.
[46] W. Yang, et al., Comparative study of the frequency-doubling performance on ring and linear cavity at short wavelength region, Opt. Express 23 (2015) 19624–19633.
[47] Y. Takeno, et al., Observation of -9 dB quadrature squeezing with improvement of phase stability in homodyne measurement, Opt. Express 15 (2007) 4321–4327.
[48] T. Serikawa, et al., Creation and measurement of broadband squeezed vacuum from a ring optical parametric oscillator, Opt. Express 24 (2016) 28383–28391.
[49] M.S. Stefszky, et al., Balanced homodyne detection of optical quantum states at audio-band frequencies and below, Class. Quantum Gravity 29 (2012) 145015.
[50] T. Tanimura, et al., Generation of a squeezed vacuum resonant on a rubidium D1 line with periodically poled $KTiOPO_4$, Opt. Lett. 31 (2006) 2344–2346.
[51] Y. Han, et al., Improvement of vacuum squeezing resonant on the rubidium D1 line at 795 nm, Opt. Express 24 (2016) 2350–2359.